ARTICLE

Enhanced performance of tin-based perovskite solar cells induced by ammonium hypophosphite additive

Received 00th January 20xx,
Accepted 00th January 20xx

DOI: 10.1039/x0xx00000x

Jiupeng Cao, Qidong Tai, Peng You, Guanqi Tang, Tianyue Wang, Naixiang Wang, Feng Yan*

As promising lead-free perovskite candidate, tin-based halide perovskites such as $FASnI_3$ have attracted extensive attention recently in photovoltaic applications. However, the relatively low efficiency and poor long-term stability of tin-based perovskite solar cells hinder their practical applications. Here, ammonium hypophosphite is introduced into the $FASnI_3$perovskite precursor to suppress the oxidation of Sn^{2+} and assist the growth of perovskite grains, leading to improved perovskite film quality and reduced defect density, and consequently, the device efficiency and open circuit voltage are substantially improved. More importantly, the solar cells exhibit pronounced enhancement of the long-term stability. This work provides a facile approach for improving the performance of tin-based perovskite solar cells by introducing ammonium hypophosphite as an antioxidant agent in the precursor solution.

Introduction

Organic-inorganic hybrid halide perovskite solar cells (PSCs) have been considered as the most promising candidate for the new generation photovoltaic technology because of their high power conversion efficiency (PCE), low cost and convenient fabrication processes[1-4].The state-of-the-art lead-based halide perovskites exhibit excellent optoelectronic properties, like strong light absorption, long carrier diffusion length and low density of defects[5-8], leading to the record PCE over 25%.[9] However, the toxic lead may cause environmental problems when PSCs are widely used. Thus, it is imperative to develop lead-free perovskites with favorable physical properties. Among various alternative metal elements (Sn, Bi, and Sb) for replacing Pb in perovskites[10-12], Sn may have the highest potential because of the ideal optical and electrical properties of tin-based perovskites for photovoltaic applications[13]. However, the device performance of tin-based PSCs still falls behind that of lead-based counterparts due to the following reasons. First, the major problem of tin-based perovskite is the poor stability because of the formation of Sn vacancies and the oxidation of Sn^{2+} to Sn^{4+}, leading to high doping levels and recombination rates in perovskite films. Second, it is difficult to get uniform and pinhole-free tin-based perovskite films due to the fast crystallization of the films[14]. So reported tin-based PSCs suffer from low efficiency and poor stability especially in air[15].

Department of Applied Physics, The Hong Kong Polytechnic University
Hung Hom, Kowloon, Hong Kong, P.R. China
**E-mail: apafyan@polyu.edu.hk*

Electronic Supplementary Information (ESI) available: [Fig. S1-S7 and Tabsle S1-S5]. See DOI: 10.1039/x0xx00000x

Tin-based PSCs have been studied by many groups and various approaches based on different principles have been developed to improve the device performance. To suppress the oxidation of Sn^{2+} and reduce the doping levels, SnF_2 or $SnCl_2$ has been incorporated into perovskite precursor solutions[16, 17]. However, an excess of SnF_2/$SnCl_2$ may cause phase separation in perovskite films (e.g. inhomogeneous dispersion) and deteriorate the device performance[18]. To further suppress the oxidation process, Kanatzidis and co-workers prepared the perovskite films under a reducing vapor atmosphere[15]. Moreover, solvent engineering[14, 19] and compositional engineering with mixed cations[20, 21] have been developed to prepare high-quality tin-based perovskite films. Very recently, tin-based perovskite film with hierarchy structure was designed to enhance oxidation resistance for improved device stability and performance[22]. However, the photovoltaic performance and stability of the tin-based PSCs still lags far behind those of lead-based PSCs. So, it is necessary to develop novel techniques that can not only retard the Sn^{2+} oxidation but also assist the preparation of compact and uniform perovskite films.

In this work, we introduced ammonium hypophosphite (AHP, $NH_4H_2PO_2$) additive in $FASnI_3$ perovskite precursor solutions for the first time. AHP is a reducing agent that can prohibit the oxidation of Sn^{2+} in perovskites[23, 24]. Meantime, $H_2PO_2^-$ can form intermediate phase with $SnCl_2$ and lead to improved film morphology and lower trap densities. In addition, we use CuSCN as a hole transporting material in the devices because of its high hole mobility and good energy alignment with $FASnI_3$. The devices show the PCE up to 7.3% with a short circuit current (J_{SC}) of 19.39 mA cm^{-2}, open circuit voltage (V_{OC}) of 0.55 V and fill factor (FF) of 68.8%. More importantly, the devices exhibit good long-term stability both in pure N_2 and ambient atmosphere. This work clearly indicates that the introduction of proper antioxidant agent in precursor solutions can boost the device performance and long-term stability of tin-based PSCs.

Experimental

Materials:

All chemicals were used as received without any further purification. Copper(I) thiocyanate (CuSCN, 99%) and $SnCl_2$ (>99%) were purchased from Sigma-Aldrich. $CH(NH_2)_2I$ was purchased from Dyesol Ltd. SnI_2 (99.999%) and phenyl-C71-butyric acid methyl ester (PCBM) were purchased from Alfa Aesar and Nano-C, respectively.

Device fabrication:

The ITO-coated glass substrates were cleaned via ultrasonication in deionized water, acetone and isopropanol for 10 min, respectively. The process of preparing CuSCN on ITO was similar with previous report[25]. CuSCN dissolved in aqueous ammonia (10 mg mL^{-1}) was spin-coated on the ITO substrate at 4000 rpm for 20 s in ambient air and then the films were annealed at 150℃ for 20 min on hotplate in air. Then the films were transferred to a nitrogen-purged glovebox for later experiment. The $FASnI_3$ perovskite precursor solution was prepared by dissolving 1 mmol SnI_2 and 1 mmol FAI with 10 mol% $SnCl_2$ in 1 mL mixed solvent (DMF:DMSO=4:1). For the AHP included perovskite precursor solution, the molar ratio of AHP and SnI_2 was 3%, 5% and 7%, respectively. The perovskite precursor solution was spin-coated on the CuSCN layer at 2000 rpm for 5 s then 5000 rpm for 30 s, and 100 µl chlorobenzene was dripped onto the perovskite film at the 11^{th} s. The obtained films were annealed at 70 ℃ for 10 min. PCBM (20 mg mL^{-1} in chlorobenzene) was spin-coated on the perovskite film at 1500 rpm for 30 s to function as electron

transporting layer. Finally, 90 nm silver electrodes were thermal evaporation on the PCBM layer under vacuum to complete the device fabrication. An active area of 0.048 cm^2 was defined by shadow mask.

Characterization:

The morphology of the films was recorded by field-emission scanning electron microscope (Hitachi S-4300). The optical absorption spectra of perovskite films were measured by Shimadzu UV-2550 spectrophotometer. XRD patterns were measured by Rigaku SmartLab X-ray diffractometer using Cu Kα radiation. The time-resolved photoluminescence (PL) spectra were obtained at 850 nm with the excitation at 650 nm by an FLS980 fluorescence spectrometer (Edinburgh Instruments, England).

The current-voltage (J-V) curves of the solar cells were measured by Keithley 2400 digital source meter under simulated air mass 1.5 G sunlight (Newport 91160, 300 W). The light intensity was calibrated by a standard monocrystalline silicon photodiode. EQE spectra were recorded by an Oriel integrated system. The Nyquist plots were recorded by a Zennium X electrochemical workstation (Zahner, Germany).

All the PSCs were measured in ambient air at room temperature without encapsulation. For the stability test, samples were stored in N_2 filled glovebox or ambient condition (~20% relative humidity) after measurements.

Results and discussion

AHP was introduced into $FASnI_3$ precursors as a reducing additive. To assess the reducing ability of AHP, a plain $FASnI_3$ precursor solution was prepared and exposed to ambient air. At the beginning, the precursor solution showed a clear yellow color (**Figure1**a). After being exposed to air for 15 minutes, the solution turned to be dark red, indicating the oxidation of Sn^{2+} to Sn^{4+}.[26] Interestingly, with the introduction of AHP (12 mol%) into the precursor solution, the color of the solution gradually changed to yellow again for the following reaction[27]

$$Sn^{4+} + 3H_2PO_2^- \rightarrow Sn^{2+} + 2HPO_3^{2-} + PH_4^+ \quad (1)$$

This result clearly indicates the reducing ability of AHP and its effect on Sn ions in the perovskite precursor.

Due to the higher Lewis acidity of Sn than that of Pb, the crystallization of Sn-based perovskite is much faster than its lead analogue, making it difficult to obtain homogeneous and compact perovskite films[28]. To evaluate the influence of AHP on the perovskite film morphology, $FASnI_3$ perovskite films prepared with various amounts of AHP were characterized under scanning electron microscopy (SEM). Many pinholes can be observed from the plain $FASnI_3$ films (**Figure 1**b) because of the fast and uncontrollable crystallization. Moreover, some needle-like aggregates formed on the film resulting from phase separation of $SnCl_2$. With the introduction of 3 mol% AHP, phase separation almost disappeared while some pinholes still existed on the film (**Figure 1**c). Notably, the inclusion of 5 mol%AHP in the precursor solution resulted in a pinhole-free and compact perovskite film (**Figure 1**d), which is beneficial for device performance. However, when the amount of AHP was increased to 7 mol%, the perovskite film became much rougher and many pinholes could be found in the film (**Figure 1**e).

Similar to our previous report[29], we consider that the AHP additive in the perovskite precursor can mix with

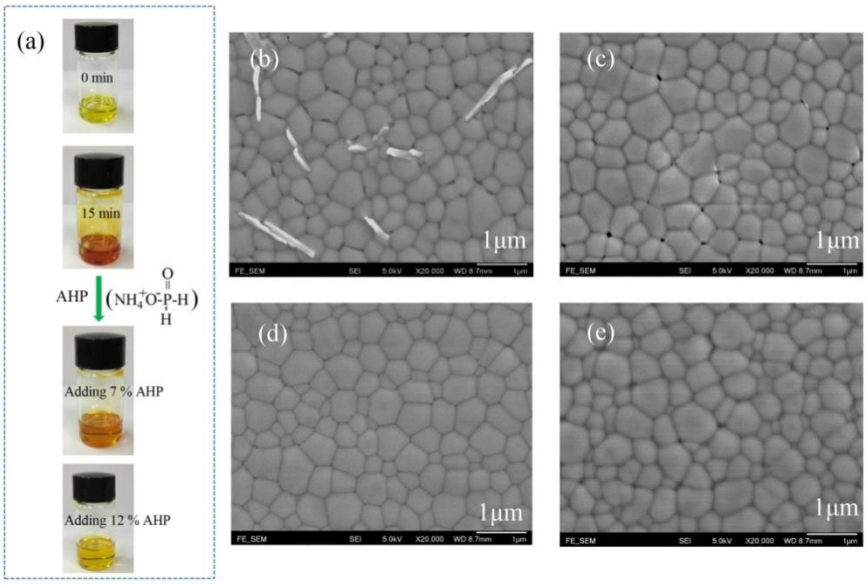

Figure1. (a) Photographs of $FASnI_3$ precursor solution and molecular structure of AHP. SEM images of $FASnI_3$ films prepared with various amounts of AHP, (b) plain $FASnI_3$, (c) 3 mol% AHP, (d) 5 mol% AHP and (e) 7 mol% AHP-added $FASnI_3$.

$SnCl_2$ and form a complex to encapsulate perovskite grains. Notably, P=O bond in AHP can coordinate with $SnCl_2$ and induce a uniform dispersion of AHP-$SnCl_2$ intermediate complex in the perovskite film and prohibit the phase separation of $SnCl_2$.[30] To confirm the interaction between AHP and $SnCl_2$, a pure AHP film and an AHP-$SnCl_2$ (molar ratio, 1:1) composite film were characterized using Fourier transform infrared spectroscopy (FTIR). As shown in **Figure 2**a, the vibration of P=O bond was shifted to an obviously lower wavenumber in the AHP-$SnCl_2$composite, which validates the strong interaction between AHP and $SnCl_2$. Meanwhile, NH_4^+ can also form intermediate phases during perovskite film preparation[31, 32]. Thus, these intermediate phases can suppress the crystallization of $SnCl_2$ and regulate the nucleation and crystallization of perovskite, resulting in a high-quality $FASnI_3$ film.

The X-ray diffraction (XRD) patterns of $FASnI_3$ films prepared with different contents of AHP are shown in **Figure S**1. The characteristic peaks of the $FASnI_3$ films without and with AHP all matched well with the orthorhombic lattice structure of $FASnI_3$. Moreover, the much sharper peaks observed from $FASnI_3$ film with 5 mol% AHP demonstrated its enhanced crystallinity. The absorption spectra of $FASnI_3$ films without and with 5 mol% AHP are shown in **Figure 2**b. All the films have similar absorption onset of ~890 nm with an estimated bandgap of 1.39 eV.

X-ray photoelectron spectroscopy (XPS) measurements were used to further evaluate the effect of AHP on the extent of Sn^{2+} oxidation in the perovskite films, and the corresponding XPS spectra are shown in **Figure S2**a,b. The 5 mol% AHP modified perovskite film showed much lower Sn^{4+} content, indicating the ability of AHP to suppress the Sn^{2+} oxidation, which is in accordance with the color change of the precursor solution (**Figure 1**a). According to **Figure S2**c, the content of Cl significantly decreased after argon etching, indicating that Cl was not incorporated into the perovskite lattice. Similar result was found for the P element from the XPS spectra (**Figure S2**d). These elemental composition values further confirm that AHP-$SnCl_2$ complex can encapsulate perovskite grains on their surfaces.

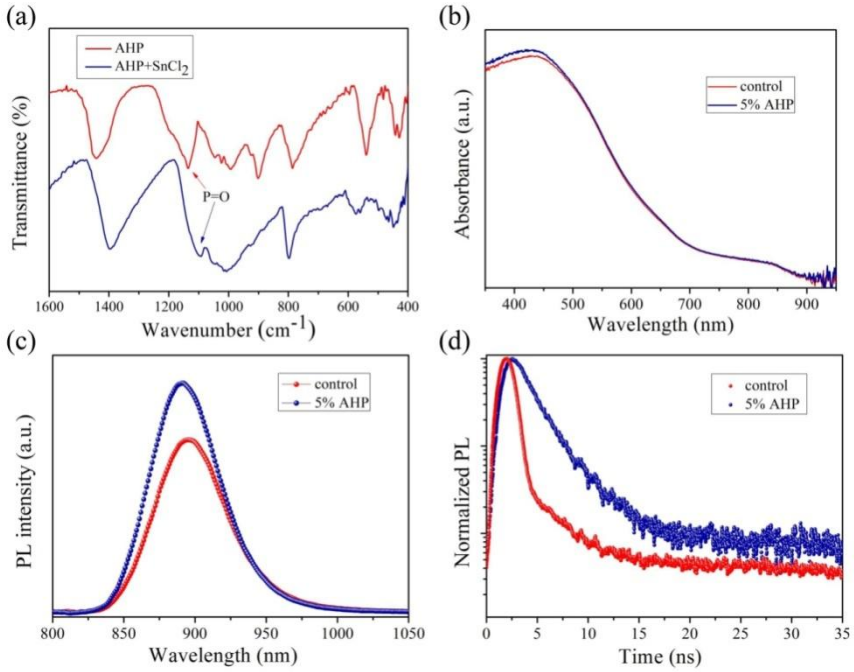

Figure 2. (a) FTIR spectra of AHP and AHP-$SnCl_2$ complex. (b) Absorption spectra of control $FASnI_3$ film and 5 mol% AHP included $FASnI_3$ film. Steady state (c) and time-resolved (d) photoluminescence spectra of plain $FASnI_3$ film and 5 mol% AHP modified $FASnI_3$ film.

To get deeper understanding of charge dynamics, the $FASnI_3$ films were characterized using steady state and time-resolved photoluminescence (PL) spectroscopy. As shown in **Figure 2**c, the plain $FASnI_3$ film showed a PL peak at around 895 nm, corresponding to a bandgap of 1.39 eV. The AHP-modified $FASnI_3$ film had a much stronger PL intensity indicating suppressed nonradiative recombination, which can be attributed to its improved film quality and reduced defect density[33]. Moreover, the blue shift of the PL peak observed in the AHP-modified $FASnI_3$ film also implied the improved crystallinity of the perovskite film. The time-resolved PL spectra are shown in **Figure 2**d, which are fitted by a bi-exponential decay model (see supporting information Table S1)[34]. The average lifetimes for the plain $FASnI_3$ film and AHP-modified $FASnI_3$ film are 0.81 ns and 2.18 ns, respectively, which further confirms the smaller trap density and reduced charge recombination induced by AHP[35, 36]. The increased carrier lifetime is favorable for the open circuit voltage of resultant PSCs[37].

Inverted PSCs with the planar device structure of ITO/CuSCN/$FASnI_3$/PCBM/Ag were prepared to evaluate the effect of AHP additive on the photovoltaic performance (**Figure S3**), and the corresponding energy diagram of the device is shown in **Figure 3**a[29, 38].The PCE statistics of $FASnI_3$ PSCs prepared with different amounts of AHP are shown in **Figure 3**b and the corresponding photovoltaic performance parameters are summarized in **Table S2**. The control devices without AHP showed average PCE of 2.34±0.71%, V_{OC} of 0.25±0.05 V, short circuit current density (J_{SC}) of 17.72±1.65 $mAcm^{-2}$ and fill factor (FF) of 51.11±9.01%. With the introduction of AHP, the device performance was improved substantially. The devices with 5 mol% AHP showed an average PCE of 6.25±0.67%, V_{OC} of 0.50±0.03 V, J_{SC} of 19.55±0.79$mAcm^{-2}$ and FF of 63.71±4.47%. As discussed before, the enhanced photovoltaic performance can be ascribed to the improved perovskite film quality and reduction of defects. However, more addition of AHP led to decreased device performance, which may come from

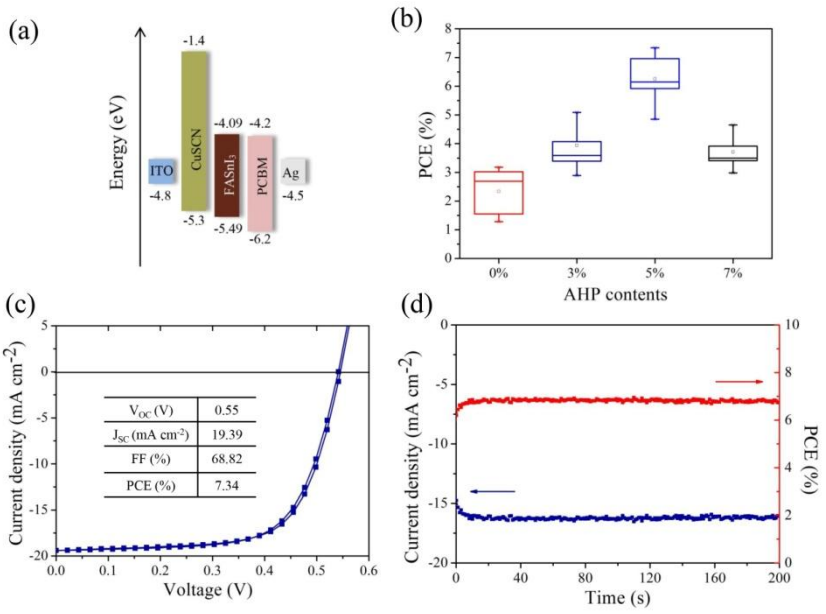

Figure3. (a) Schematic energy diagram of the $FASnI_3$ solar cells. (b) The PCE distribution of $FASnI_3$ solar cells prepared with various contents of AHP. (c) Current density-voltage (J-V) curve of the champion device. (d) Stabilized PCE and photocurrent density of the champion device measured at a bias of 0.43 V.

deteriorated perovskite films with pinholes and high roughness.

The current density-voltage (J-V) curve of the champion PSC (5 mol% AHP) is shown in **Figure 3**c, achieving a PCE of 7.34% and V_{OC} of 0.55 V with negligible hysteresis. To verify the reliability of the device performance, the stabilized photocurrent and power output were measured at a bias of 0.43 V under AM 1.5 G illumination. As shown in **Figure 4**d, a stabilized output power of ~7.0% was achieved, which is close to the value obtained from the J-V curve. Notably, the V_{OC} up to 0.55 V is among the highest value for $FASnI_3$ based PSCs (**Table S3**), which can be attributed to decreased defect density in perovskite film and the good energy alignment between perovskite and the hole transporting material CuSCN[38, 39].The external quantum efficiency (EQE) spectrum of the champion device is shown in **Figure S4**, and the integrated current density is 18.8 mA cm^{-2}, which is close to the value measured from the J-V curve (Figure 3c). Moreover, the photovoltaic parameters of control and 5 mol% AHP-modified devices are shown in **Figure S5**. The results clearly indicate that the introduction of AHP can improve both the reproducibility and efficiency of the devices.

To evaluate the charge transport properties of the devices, we measured the dark current density[40], as shown in **Figure 4**a. The plain $FASnI_3$ solar cells suffered from high leakage current because of the highly p-type doping. On the contrary, the 5 mol% AHP modified $FASnI_3$ solar cells showed good diode behavior with almost 1-2 orders lower leakage current than that of the control one, indicating its much reduced background carrier density[41]. We further measured the trap state density in the perovskite absorber by the space charge limited current (SCLC) method[42]. Electron-only devices with a structure of ITO/SnO_2/perovskite/PCBM/Ag were prepared to get dark J-V curves, as shown in **Figure 4**b. At low bias voltages, the J-V curves show linear relation, corresponding to the Ohmic region. With the bias voltage exceeding the kink point, the current density quickly increases, implying that the trap states are fully filled. Using the trap-filled limit

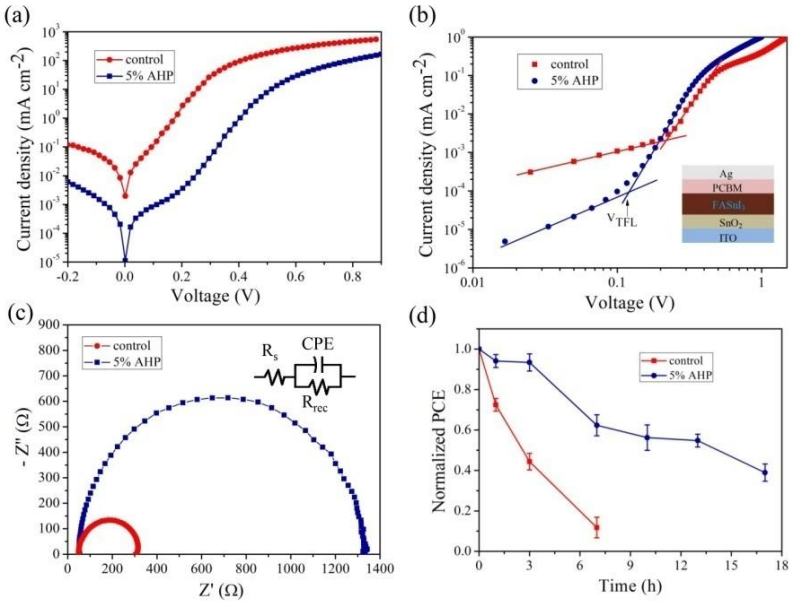

Figure 4.(a) J-V curves of $FASnI_3$ solar cells with and without AHP measured in dark. (b) J-V curves of electron-only devices. The insert shows the device structure. (c) Nyquist plots of $FASnI_3$ solar cells with and without AHP (inset gives the equivalent circuit for fitting). (d) Light soaking test of unencapsulated $FASnI_3$ solar cells under 100 mw cm^{-2} white light illumination in air with ~20% humidity.

voltage (V_{TFL}), we can obtain the trap state density N_t by this equation:

$$N_t=2\varepsilon\varepsilon_0 V_{TFL}/qL^2, \quad (2)$$

where ε and ε_0 are the relative and vacuum dielectric constants, respectively, q is the elementary charge and L is the thickness of the perovskite film[43, 44]. The V_{TFL} of the control and AHP-included devices are around 0.22 V and 0.12 V, corresponding to trap state densities of 3.45×10^{15} cm^{-3} and 1.88×10^{15} cm^{-3}, respectively. The much lower trap state density of the AHP-modified perovskite film is favorable for the device performance.

To get further insight into the charge transport characteristics of the solar cells, electrochemical impedance spectroscopy of the PSCs was recorded[45, 46]. **Figure 4**c shows the Nyquist plots of the $FASnI_3$ solar cells without and with 5 mol% AHP addition, which were recorded at a bias of 0.3 V in dark. Generally, the semicircle at low frequency can be attributed to the recombination resistance (R_{rec}) and constant phase element (CPE), and the charge recombination rate is inversely proportional to recombination resistance[47-50]. The R_{rec} values for the control and AHP-modified solar cells measured at different bias voltages are shown in **Figure S6** and **Table S4**.The AHP–modified device had a much bigger R_{rec}, indicating a much lower recombination rate than that in the control.

The stability of the unencapsulated $FASnI_3$ PSCs under light soaking test is presented in **Figure 4**d. In previous reports, the unencapsulated devices degraded quickly in ambient air (**Table S5**). More than 60% of its original PCE was maintained after 10 h while the control devices degraded rapidly within 6 h because of the easy oxidation of Sn^{2+}. We also examined the storage stability of the devices both in air and N_2-filled glovebox (without encapsulation), as shown in **Figure S7**. In air, about 50% of its original PCE was maintained after the storage for 500 h while the control devices degraded rapidly within 100 h. When stored in N_2 environment, the devices with 5 mol% AHP could maintain 70% of their original PCE over 1000 h, while the control devices degraded more quickly and maintained only 50% of the initial PCE in the same period.

The enhanced long-term stability induced by AHP can be ascribed to the reducing effect of AHP around the perovskite grains as well as the compact and pinhole free film morphology that can effectively suppress the permeation of oxygen.

Conclusion

In summary, AHP was introduced into the perovskite precursor to suppress the oxidation of Sn^{2+} and retard the fast crystallization of $FASnI_3$. This method can substantially improve the film quality and decrease the trap density in the perovskite films. Meantime, inorganic CuSCN was used as hole transporting material for $FASnI_3$ PSCs to form good energy level alignment of the devices[51]. Consequently, improved photovoltaic performance was obtained in the resultant PSCs. Moreover, the AHP-included $FASnI_3$ PSCs demonstrate outstanding long term stability both in N_2 and ambient condition. Our work suggests that the combination of effective antioxidant additive and suitable hole extraction layer can improve the photovoltaic performance as well as the long-term stability of tin-based PSCs.

Conflicts of interest

The authors declare no competing financial interest.

Acknowledgements

This work was financially supported by the Research Grants Council (RGC) of Hong Kong, China (Project No. PolyU 152068/18E).

Notes and references

1. A. Kojima, K. Teshima, Y. Shirai and T. Miyasaka, *Journal of the American Chemical Society*, 2009, **131**, 6050-6051.
2. H.-S. Kim, C.-R. Lee, J.-H. Im, K.-B. Lee, T. Moehl, A. Marchioro, S.-J. Moon, R. Humphry-Baker, J.-H. Yum, J. E. Moser, M. Grätzel and N.-G. Park, *Scientific Reports*, 2012, **2**, 591.
3. W. S. Yang, B.-W. Park, E. H. Jung, N. J. Jeon, Y. C. Kim, D. U. Lee, S. S. Shin, J. Seo, E. K. Kim, J. H. Noh and S. I. Seok, *Science*, 2017, **356**, 1376-1379.
4. M. A. Green, A. Ho-Baillie and H. J. Snaith, *Nature Photonics*, 2014, **8**, 506.
5. M. B. Johnston and L. M. Herz, *Accounts of Chemical Research*, 2016, **49**, 146-154.
6. P. You, Z. Liu, Q. Tai, S. Liu and F. Yan, *Advanced materials*, 2015, **27**, 3632-3638.
7. Q. Tai, P. You, H. Sang, Z. Liu, C. Hu, H. L. W. Chan and F. Yan, *Nature communications*, 2016, **7**, 11105.
8. Z. Liu, P. You, C. Xie, G. Tang and F. Yan, *Nano Energy*, 2016, **28**, 151-157.
9. NREL Efficiency Chart (Sep. 2019), https://www.nrel.gov/pv/assets/pdfs/best-research-cell-efficiencies.20190802.pdf).
10. B.-W. Park, B. Philippe, X. Zhang, H. Rensmo, G. Boschloo and E. M. J. Johansson, *Advanced materials*, 2015, **27**, 6806-6813.
11. R. Nie, A. Mehta, B.-w. Park, H.-W. Kwon, J. Im and S. I. Seok, *Journal of the American Chemical Society*, 2018, **140**, 872-875.
12. F. Hao, C. C. Stoumpos, D. H. Cao, R. P. H. Chang and M. G. Kanatzidis, *Nature Photonics*, 2014, **8**, 489-494.
13. W. Ke, C. C. Stoumpos and M. G. Kanatzidis, *Advanced materials*, **0**, 1803230.
14. F. Hao, C. C. Stoumpos, P. Guo, N. Zhou, T. J. Marks, R. P. H. Chang and M. G. Kanatzidis, *Journal of the American Chemical Society*, 2015, **137**, 11445-11452.
15. T.-B. Song, T. Yokoyama, C. C. Stoumpos, J. Logsdon, D. H. Cao, M. R. Wasielewski, S. Aramaki and M. G. Kanatzidis, *Journal of the American Chemical Society*, 2017, **139**, 836-842.
16. K. M. Hemant, D. Sabba, L. W. Lin, B. P. P., P. R. Ramanujam, B. Tom, S. Chen, D. Hong, R. Ramamoorthy, A. Mark, G. Michael, M. S. G. and M. Nripan, *Advanced materials*, 2014, **26**, 7122-7127.
17. W. Liao, D. Zhao, Y. Yu, C. R. Grice, C. Wang, A. J. Cimaroli, P. Schulz, W. Meng, K. Zhu, R.-G. Xiong and Y. Yan, *Advanced materials*, 2016, **28**, 9333-9340.
18. S. J. Lee, S. S. Shin, Y. C. Kim, D. Kim, T. K. Ahn, J. H. Noh, J. Seo and S. I. Seok, *Journal of the American Chemical Society*, 2016, **138**, 3974-3977.
19. X. Liu, K. Yan, D. Tan, X. Liang, H. Zhang and W. Huang, *ACS Energy Letters*, 2018, **3**, 2701-2707.
20. Z. Zhao, F. Gu, Y. Li, W. Sun, S. Ye, H. Rao, Z. Liu, Z. Bian and C. Huang, *Advanced Science*, 2017
21. W. Ke, C. C. Stoumpos, M. Zhu, L. Mao, I. Spanopoulos, J. Liu, O. Y. Kontsevoi, M. Chen, D. Sarma and Y. Zhang, *Science Advances*, 2017, **3**, e1701293.
22. F. Wang, X. Jiang, H. Chen, Y. Shang, H. Liu, J. Wei, W. Zhou, H. He, W. Liu and Z. Ning, *Joule*, 2018
23. W. Zhang, S. Pathak, N. Sakai, T. Stergiopoulos, P. K. Nayak, N. K. Noel, A. A. Haghighirad, V. M. Burlakov, A. Sadhanala and W. Li, *Nature communications*, 2015, **6**, 10030.
24. W. Li, J. Li, J. Li, J. Fan, Y. Mai and L. Wang, *Journal of Materials Chemistry A*, 2016, **4**, 17104-17110.
25. N. Wijeyasinghe, A. Regoutz, F. Eisner, T. Du, L. Tsetseris, Y.-H. Lin, H. Faber, P. Pattanasattayavong, J. Li, F. Yan, M.

A. McLachlan, D. J. Payne, M. Heeney and T. D. Anthopoulos, *Advanced Functional Materials*, 2017, **27**, 1701818.
26. F. Gu, S. Ye, Z. Zhao, H. Rao, Z. Liu, Z. Bian and C. Huang, *Solar RRL*, 2018, **2**, 1800136.
27. W. Xu, G. Lei, C. Tao, J. Zhang, X. Liu, X. Xu, W.-Y. Lai, F. Gao and W. Huang, *Advanced Functional Materials*, 2018, **28**, 1802320.
28. Z. Zhu, C.-C. Chueh, N. Li, C. Mao and A. K. Y. Jen, *Advanced materials*, 2018, **30**, 1703800.
29. Q. Tai, X. Guo, G. Tang, P. You, T.-W. Ng, D. Shen, J. Cao, C.-K. Liu, N. Wang, Y. Zhu, C.-S. Lee and F. Yan, *Angewandte Chemie International Edition*, 2019, **58**, 806-810.
30. X. Yang, X. Zhang, J. Deng, Z. Chu, Q. Jiang, J. Meng, P. Wang, L. Zhang, Z. Yin and J. You, *Nature communications*, 2018, **9**, 570.
31. H. Si, Q. Liao, Z. Kang, Y. Ou, J. Meng, Y. Liu, Z. Zhang and Y. Zhang, *Advanced Functional Materials*, 2017, **27**, 1701804.
32. C. Zuo, D. Vak, D. Angmo, L. Ding and M. Gao, *Nano Energy*, 2018, **46**, 185-192.
33. G. Tang, P. You, Q. Tai, R. Wu and F. Yan, *Solar RRL*, 2018, **2**, 1800066.
34. G. Tang, P. You, Q. Tai, A. Yang, J. Cao, F. Zheng, Z. Zhou, J. Zhao, P. K. L. Chan and F. Yan, *Advanced materials*, 2019, **31**, 1807689.
35. W. Ke, C. C. Stoumpos, I. Spanopoulos, L. Mao, M. Chen, M. R. Wasielewski and M. G. Kanatzidis, *Journal of the American Chemical Society*, 2017, **139**, 14800-14806.
36. E. Jokar, C.-H. Chien, C.-M. Tsai, A. Fathi and E. W.-G. Diau, *Advanced materials*, **0**, 1804835.
37. S. Shao, M. Abdu-Aguye, T. S. Sherkar, H.-H. Fang, S. Adjokatse, G. t. Brink, B. J. Kooi, L. J. A. Koster and M. A. Loi, *Advanced Functional Materials*, 2016, **26**, 8094-8102.
38. J. W. Jung, C.-C. Chueh and A. K.-Y. Jen, *Advanced Energy Materials*, 2015, **5**, 1500486.
39. X. Liu, Y. Wang, F. Xie, X. Yang and L. Han, *ACS Energy Letters*, 2018, **3**, 1116-1121.
40. Q. Wang, Y. Shao, Q. Dong, Z. Xiao, Y. Yuan and J. Huang, *Energy & environmental science*, 2014, **7**, 2359-2365.
41. C. He, C. Zhong, H. Wu, R. Yang, W. Yang, F. Huang, G. C. Bazan and Y. Cao, *Journal of Materials Chemistry*, 2010, **20**, 2617-2622.
42. W. Ke, C. C. Stoumpos, I. Spanopoulos, L. Mao, M. Chen, M. R. Wasielewski and M. G. Kanatzidis, *Journal of the American Chemical Society*, 2017, **139**, 14800-14806.
43. D. Yang, X. Zhou, R. Yang, Z. Yang, W. Yu, X. Wang, C. Li, S. Liu and R. P. H. Chang, *Energy & environmental science*, 2016, **9**, 3071-3078.
44. C. Ran, J. Xi, W. Gao, F. Yuan, T. Lei, B. Jiao, X. Hou and Z. Wu, *ACS Energy Letters*, 2018, **3**, 713-721.
45. Q. Tai, X. Zhao and F. Yan, *Journal of Materials Chemistry*, 2010, **20**, 7366-7371.
46. G. Liu, C. Zhou, F. Wan, K. Li, Y. Yuan, Y. Gao, Y. Lu and B. Yang, *Applied Physics Letters*, 2018, **113**, 113501.
47. W. Ke, C. C. Stoumpos, I. Spanopoulos, M. Chen, M. R. Wasielewski and M. G. Kanatzidis, *ACS Energy Letters*, 2018, **3**, 1470-1476.
48. A. K. Chandiran, A. Yella, M. T. Mayer, P. Gao, M. K. Nazeeruddin and M. Grätzel, *Advanced materials*, 2014, **26**, 4309-4312.
49. E. J. Juarez-Perez, M. Wuβler, F. Fabregat-Santiago, K. Lakus-Wollny, E. Mankel, T. Mayer, W. Jaegermann and I. Mora-Sero, *The journal of physical chemistry letters*, 2014, **5**, 680-685.
50. Q. Tai, K.-C. Tang and F. Yan, *Energy & environmental science*, 2019, **12**, 2375-2405.
51. J. Chen and N.-G. Park, *The Journal of Physical Chemistry C*, 2018, **122**, 14039-14063.